Progress In Electromagnetics Research M, Vol. 119, 25–35, 2023

$\mathcal{H}$-Matrix Solver for the Acceleration of Boundary Integral Equation for Photonic Crystal Fiber

Jean-René Poirier[1, *], Julien Vincent[2], Priscillia Daquin[1, 3], Ronan Perrussel[1], and Han Cheng Seat[4]

Abstract—A waveguide mode solver based on boundary integral equation (BIE) method and matrix compression is developed in this study. Using an accurate discretization based on a Nyström method and a kernel-splitting technique, the BIE method gives rise to three different formulations of a nonlinear eigenvalue problem. $\mathcal{H}$-matrices are used in order to accelerate and increase the precision of the subsequent computations. Results from these investigations on a canonical photonic crystal fiber (PCF) chosen as an example demonstrate that the data sparse representation of the BIE discretization reduces the memory storage, as well as the assembly and solution times.

1. INTRODUCTION

Photonic crystal fibers (PCFs) are complex systems that have been increasingly exploited over the past two decades in optoelectronic systems to enhance the propagation of light [1, 2]. The geometry of these optical waveguides, together with the dielectric characteristics of the materials and the wavelength of the light source traveling through the fiber define the essential parameters for the propagation of information. These parameters are used to determine the effective refractive index, which can be a complex number. Resolving the complexity of these optical systems — heterogeneous structure, geometry of the waveguide section, and micrometric order of magnitude — thus requires powerful optimized numerical methods and tools in electromagnetism for the rapid design of PCFs for the desired application.

The finite-difference time-domain (FDTD) method and the finite element method (FEM) are the most common approaches used to solve the problem of PCF propagation [3–5]. However, both FDTD and FEM may require a huge amount of memory and computation time, as a function of the mesh size for a PCF with many microstructures. More specific techniques such as a modal approach [6], a particular Green function [7] or the multipole method [8] can also be considered for this problem, but they are often limited to some types of inclusions (circular for instance). More recently, some tools based on the boundary element method (BEM) [9, 10] have been proposed which can allow to consider only the mesh on the boundary of the inclusions. Furthermore, the BEM can now generally be improved with compression techniques such as the fast multipole method [11] or the hierarchical matrices ($\mathcal{H}$-matrices) [12, 13].

The main novelty of this work lies in the adaptation of these compression techniques to the peculiarities of the BEM applied to the PCF discretization [9, 10], namely the particular block structure of the matrix of the problem and the multiple solutions due to the numerical method [14] required to deal with the nonlinearity of the problem.

The paper is organized as follows. Section 2 is devoted to the description of the BEM formulation of the PCF problem modeling. In Section 3, the theory of $\mathcal{H}$-matrices is introduced for reducing memory

Received 24 March 2023, Accepted 10 July 2023, Scheduled 14 September 2023
* Corresponding author: Jean-René Poirier (poirier@laplace.univ-tlse.fr).
[1] LAPLACE, University of Toulouse, CNRS, INPT, UPS, Toulouse, France. [2] MBDA Missile Systems, France. [3] CNES, Toulouse, France. [4] LAAS-CNRS, Université de Toulouse, CNRS, INP, Toulouse, France.

storage and accelerating the solution. In Section 4, the validity and efficiency of several strategies are studied. Finally, the method is applied to determine the effective refractive index for the chosen example with high accuracy.

2. PROBLEM FORMULATION

2.1. Maxwell's Equations and Transmission Conditions

Let us consider a PCF invariant along the z-direction with C homogeneous inclusions $(\Omega_j)_{j=1,\dots,C}$ with the refractive index (RI) n_j, embedded in a homogeneous infinite background material Ω_0 with RI n_0. The dependence of the electromagnetic field in z is then taken into account by a term $\exp(\mathrm{i}\beta z)$ meaning an $\exp(-\mathrm{i}\omega t)$ dependence with i the imaginary unit and β a propagation constant. Normal and tangential vectors to the boundaries are respectively denoted by $\boldsymbol{\nu}$ and $\boldsymbol{\tau}$. Figure 1 is an example of a three-inclusions PCF with such notations ($C = 3$, $j = 1, 2, 3$).

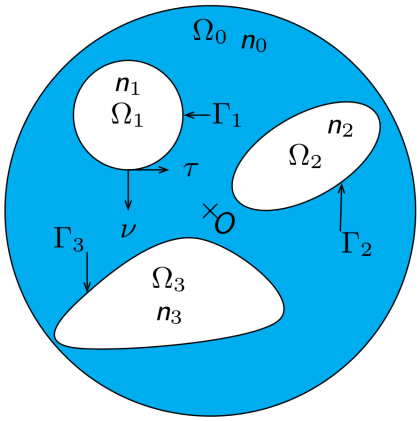

Figure 1. Representation of a three-inclusions PCF with associated notations.

In the transverse plan $(O, \mathbf{x}, \mathbf{y})$, the electric field $\mathbf{E}$ and the magnetic field $\mathbf{H}$ satisfy the Helmholtz equation. Moreover, the interface conditions relate the RIs to the tangential and normal derivatives of the tangential components of the electromagnetic field. In the following, the scalar unknowns E and H refer to the z-components of the electromagnetic field such that $E = E_z$ and $H = \sqrt{\frac{\mu_0}{\varepsilon_0}} H_z$. Equations (1) and (2) are satisfied in each Ω_j, and transmission conditions across boundaries Γ_j are defined by Equations (3) to (6); see also [16].

$$\left[\nabla^2 + (k^2 - \beta^2)\right] E = 0, \text{ in } \Omega_j, \forall j \in [\![1; C]\!], \tag{1}$$

$$\left[\nabla^2 + (k^2 - \beta^2)\right] H = 0, \text{ in } \Omega_j, \forall j \in [\![1; C]\!], \tag{2}$$

$$[E]_{\Gamma_j} = 0, \ \forall j \in [\![1; C]\!], \tag{3}$$

$$[H]_{\Gamma_j} = 0, \ \forall j \in [\![1; C]\!], \tag{4}$$

$$\left[\frac{n_{\mathit{eff}}}{n_j^2 - n_{\mathit{eff}}^2} \frac{\partial E}{\partial \boldsymbol{\tau}}\right]_{\Gamma_j} = \left[\frac{1}{n_j^2 - n_{\mathit{eff}}^2} \frac{\partial H}{\partial \boldsymbol{\nu}}\right]_{\Gamma_j}, \ \forall j \in [\![1; C]\!], \tag{5}$$

$$\left[\frac{n_{\mathit{eff}}}{n_j^2 - n_{\mathit{eff}}^2} \frac{\partial H}{\partial \boldsymbol{\tau}}\right]_{\Gamma_j} = -\left[\frac{n_j^2}{n_j^2 - n_{\mathit{eff}}^2} \frac{\partial E}{\partial \boldsymbol{\nu}}\right]_{\Gamma_j}, \ \forall j \in [\![1; C]\!], \tag{6}$$

where $[E]_{\Gamma_j}$ represents the jump of E across Γ_j; n_j is the RI in the domain Ω_j; $k = k_0 n_j$ is the wavenumber in Ω_j; and $k_0 = 2\pi/\lambda_0$ is the free space wavenumber. The propagation of light inside the

PCF is determined by the value of β which can be complex. The imaginary part of β can be very small for leaky modes. Accurate solvers are therefore needed to compute the effective RI n_{eff}, with $n_{eff} = k_0/\beta$.

2.2. BIE Method for the PCF

In this section, a PCF is described with C homogeneous inclusions with the same RI n_i, embedded in an infinite medium Ω_0 with RI n_0. On the interfaces $\partial\Omega_j$, the single and double layer potentials inside and outside the inclusions give the relations between the electric and magnetic fields, and their normal derivatives through the Green function G defined by

$$G(\mathbf{r},\tilde{\mathbf{r}}) = \frac{\mathrm{i}}{4} H_0^{(1)}\left((k^2-\beta^2)|\mathbf{r}-\tilde{\mathbf{r}}|\right), \quad \mathbf{r} \neq \tilde{\mathbf{r}} \tag{7}$$

where $H_0^{(1)}$ is a Hankel function. The field $u = E$ or H can be given by the representation formula [9, 10]

$$u(\mathbf{r}) = \pm\left(\int_{\partial\Omega_j} G(\mathbf{r},\tilde{\mathbf{r}})\frac{\partial u(\tilde{\mathbf{r}})}{\partial \boldsymbol{\nu}}\,\mathrm{d}s(\tilde{\mathbf{r}}) - \int_{\partial\Omega_j}\frac{\partial G(\mathbf{r},\tilde{\mathbf{r}})}{\partial \boldsymbol{\nu}(\tilde{\mathbf{r}})}\,u(\tilde{\mathbf{r}})\mathrm{d}s(\tilde{\mathbf{r}})\right), \ \ \mathbf{r} \notin \partial\Omega_j, \tag{8}$$

where the $\pm$ sign corresponds respectively to the interior and exterior domains. Using the properties of the single and double layer potentials when $\mathbf{r}$ tends to $\partial\Omega_j$, we obtain the following integral equation to express the normal derivative of u

$$\frac{\partial u(\mathbf{r})}{\partial \boldsymbol{\nu}} = \frac{1}{2}\frac{\partial u(\mathbf{r})}{\partial \boldsymbol{\nu}} \pm \left(\int_{\partial\Omega_j}\frac{\partial G(\mathbf{r},\tilde{\mathbf{r}})}{\partial \boldsymbol{\nu}(\mathbf{r})}\frac{\partial u(\tilde{\mathbf{r}})}{\partial \boldsymbol{\nu}}\,\mathrm{d}s(\tilde{\mathbf{r}}) - \int_{\partial\Omega_j}\frac{\partial^2 G(\mathbf{r},\tilde{\mathbf{r}})}{\partial \boldsymbol{\nu}(\tilde{\mathbf{r}})\partial \boldsymbol{\nu}(\mathbf{r})}\,u(\tilde{\mathbf{r}})\mathrm{d}s(\tilde{\mathbf{r}})\right), \ \ \mathbf{r} \in \partial\Omega_j.$$

Using the notations $u = E = \mu_i^E$ for the interior field on any boundary $\partial\Omega_j$ and $\sigma_i^E = \frac{\partial u}{\partial \boldsymbol{\nu}_i}(\mathbf{r})$ for the corresponding inside derivative, we can rewrite this equation in terms of operators

$$\left(\frac{1}{2}\,Id - J_i\right)\sigma_i^E = -W_i\mu_i^E \quad \text{on any } \partial\Omega_j \tag{9}$$

where Id is the identity operator, and J_i and W_i are the following singular operators

$$\begin{cases} (J_i\psi)(\mathbf{r}) = \displaystyle\int_{\partial\Omega_j}\frac{\partial G(\mathbf{r},\tilde{\mathbf{r}})}{\partial \boldsymbol{\nu}(\mathbf{r})}\,\psi(\tilde{\mathbf{r}})\,\mathrm{d}s(\tilde{\mathbf{r}}), \ \ \mathbf{r} \in \partial\Omega_j, \\ (W_i\psi)(\mathbf{r}) = \displaystyle\int_{\partial\Omega_j}\frac{\partial^2 G(\mathbf{r},\tilde{\mathbf{r}})}{\partial \boldsymbol{\nu}(\mathbf{r})\partial \boldsymbol{\nu}(\tilde{\mathbf{r}})}\,\psi(\tilde{\mathbf{r}})\,\mathrm{d}s(\tilde{\mathbf{r}}), \ \ \mathbf{r} \in \partial\Omega_j. \end{cases} \tag{10}$$

With similar notations $u = E = \mu_e^E$ for the outside field on any boundary $\partial\Omega_j$, and $\sigma_e^E = \frac{\partial u}{\partial \boldsymbol{\nu}_e}(\mathbf{r})$ for the corresponding outside derivative, we define the boundary integral equation as

$$(Id + J_e)\sigma_e^E = W_e\mu_e^E \quad \text{on any } \partial\Omega_j. \tag{11}$$

In the background material Ω_0, all inclusions interact with the others, and J_e and W_e are therefore provided by

$$\begin{cases} (J_e\psi)(\mathbf{r}) = \displaystyle\sum_{l=1}^{C}\int_{\partial\Omega_l}\frac{\partial G(\mathbf{r},\tilde{\mathbf{r}})}{\partial \boldsymbol{\nu}(\mathbf{r})}\,\psi(\tilde{\mathbf{r}})\,\mathrm{d}s(\tilde{\mathbf{r}}), \\ (W_e\psi)(\mathbf{r}) = \displaystyle\sum_{l=1}^{C}\int_{\partial\Omega_l}\frac{\partial^2 G(\mathbf{r},\tilde{\mathbf{r}})}{\partial \boldsymbol{\nu}(\mathbf{r})\partial \boldsymbol{\nu}(\tilde{\mathbf{r}})}\,\psi(\tilde{\mathbf{r}})\,\mathrm{d}s(\tilde{\mathbf{r}}). \end{cases} \tag{12}$$

Similar equations can also be derived for the field $u = H$.

To express the transmission conditions (5) and (6), we also consider the discretized tangential operator $T \sim \partial_\tau$. We can now provide the expression of the complete problem using Equations (9) and (11), and the transmission condition (3) to obtain

$$\mu_i^E = \mu_e^E = \mu^E \Rightarrow \left(\frac{1}{2}\,Id - J_i\right)\sigma_i^E = -W_i\mu^E \ \text{ and } \ (Id + J_e)\,\sigma_e^E = W_e\mu^E,$$

and the transmission condition (4) to obtain

$$\mu_i^H = \mu_e^H = \mu^H \Rightarrow \left(\frac{1}{2}Id - J_i\right)\sigma_i^H = -W_i\mu^H \text{ and } (Id + J_e)\sigma_e^H = W_e\mu^H,$$

as well as the transmission conditions (5) and (6) to further obtain

$$\begin{aligned} c_0\sigma_i^E - c_1\sigma_e^E &= c_2 T\mu^H, \\ c_3\sigma_i^H - c_4\sigma_e^H &= c_2 T\mu^E. \end{aligned}$$

In the above equations, the constants c_i, $i \in [\![1;5]\!]$ are defined by

$$\begin{cases} c_0 = -\dfrac{n_i^2}{n_i^2 - n_{\mathit{eff}}^2}, \quad c_1 = \dfrac{n_0^2}{n_0^2 - n_{\mathit{eff}}^2}, \quad c_2 = \left(\dfrac{n_{\mathit{eff}}}{n_0^2 - n_{\mathit{eff}}^2} - \dfrac{n_{\mathit{eff}}}{n_i^2 - n_{\mathit{eff}}^2}\right) \\ c_3 = \dfrac{1}{n_i^2 - n_{\mathit{eff}}^2} = \dfrac{k_0^2}{k_i^2}, \quad c_4 = -\dfrac{1}{n_0^2 - n_{\mathit{eff}}^2} = -\dfrac{k_0^2}{k_e^2}. \end{cases}$$

2.3. The Nonlinear Algebraic Problem

Using an accurate discretization based on the Nyström method [9, 10] and a kernel-splitting technique [15], we obtain a linear system represented by a block matrix. We denote B_1 the discretization of $(Id - J_i)$ and B_2 the discretization of $(Id + J_e)$. Note also that B_1 is a block diagonal matrix with C separated blocks, and B_2 is *a priori* a full matrix. If we keep the same notations, W_e, W_i, and T are now discrete counterparts of the corresponding integral or differential operators, and in the same way, we have discrete counterparts of respectively μ^E, σ_i^E, σ_e^E, μ^H, σ_i^H, and σ_e^H. Using the substitutions

$$\sigma_e^E = \frac{c_0}{c_1}\,\sigma_i^E - \frac{c_2}{c_1}\,T\mu^H \quad \text{and} \quad \sigma_e^H = \frac{c_2}{c_4}\,T\mu^E - \frac{c_3}{c_4}\,\sigma_i^H,$$

we obtain a reduced linear system

$$\begin{bmatrix} W_e & -\dfrac{c_0}{c_1}B_2 & \dfrac{c_2}{c_1}B_3 & 0 \\ W_i & B_1 & 0 & 0 \\ \dfrac{c_2}{c_4}B_3 & & W_e & -\dfrac{c_3}{c_4}B_2 \\ 0 & 0 & W_i & B_1 \end{bmatrix} \cdot \begin{bmatrix} \mu^E \\ \sigma_i^E \\ \mu^H \\ \sigma_i^H \end{bmatrix} = 0. \tag{13}$$

where $B_3 = B_2T$.

This system (13) requires a full but compressed matrix (as detailed in Subsection 3.1) in the product $B_3 = B_2T$, and the resulting matrix is of the same structure. The resulting linear system is reduced to 4 unknowns with an additional cost for assembling the matrix.

Another approach provides a 2×2 block matrix, using

$$W_i\mu^E = -B_1\sigma_i^E \text{ and } W_i\mu^H = -B_1\sigma_i^H,$$

and this then leads to

$$\begin{bmatrix} W_e + \dfrac{c_0}{c_1}B_2B_1^{-1}W_i & \dfrac{c_2}{c_1}B_3 \\ \dfrac{c_2}{c_4}B_3 & W_e + \dfrac{c_3}{c_4}B_2B_1^{-1}W_i \end{bmatrix} \cdot \begin{bmatrix} \mu^E \\ \mu^H \end{bmatrix} = 0. \tag{14}$$

This step requires inverting a block matrix with sparse part and two additional matrix/matrix products, but the size of the linear system to solve is reduced by half.

In both cases, the final system is a problem that can be expressed in the form

$$F(n_{\mathit{eff}})\mathbf{\Psi} = 0. \tag{15}$$

Equation (15) gives rise to a nonlinear eigenvalue problem to solve. For a given complex value n_{eff}, a mode of the PCF is determined by the point where the matrix F becomes singular. Following [9],

finding all modes of the PCF consists in seeking the zeros of a function f defined by (16) where $\boldsymbol{\phi}$ and $\boldsymbol{\psi} \in \mathbb{C}^{n\times p}$ are two random complex rectangular matrices.

$$f(n_{eff}) = \frac{1}{\|\boldsymbol{\phi}^T F^{-1}(n_{eff})\boldsymbol{\psi}\|_2}. \tag{16}$$

The zeros can be found by the Muller method. Numerically, computation of $F^{-1}(n_{eff})\boldsymbol{\psi}$ consists in solving a linear system with several right-hand sides. Consequently, a limitation of this approach in terms of compression tools like $\mathcal{H}$-matrix will be the fact that near the solution, $F(n_{eff})$ is singular and may be strongly affected by the approximation.

We will thus employ an approach based on contour integral (CI), as described in [14]. In both methods (Muller and CI), the problem will consist in solving the same linear system already defined by the matrix F and a random right-hand side, but in the CI method, we only need to compute for a set of value s (typically 5 to 20) of n_{eff} that are not in the vicinity of the roots of F.

3. ASSEMBLY OF THE PROBLEM IN $\mathcal{H}$-MATRIX FORMAT

3.1. $\mathcal{H}$-Matrix

3.1.1. Clustering and $\mathcal{H}$-Matrix

Let us first recall the general principles of hierarchical matrices for integral equations (IEs). The first step consists in a hierarchical subdivision of the geometry of the target under investigation into particular regions. Due to the IEs, two regions have interactions that are represented by particular blocks in the matrix after discretization. Some of these blocks have compression properties, i.e., they can be approximated by low-rank matrices. In this work, Adaptive Cross Approximation (ACA) is performed to build the low-rank matrices. The accuracy of this approximation is controlled by a threshold parameter ϵ_{ACA}. The distribution of the blocks is obtained thanks to a hierarchical division of the geometry (clustering) by a binary tree, as shown in Figure 2(a).

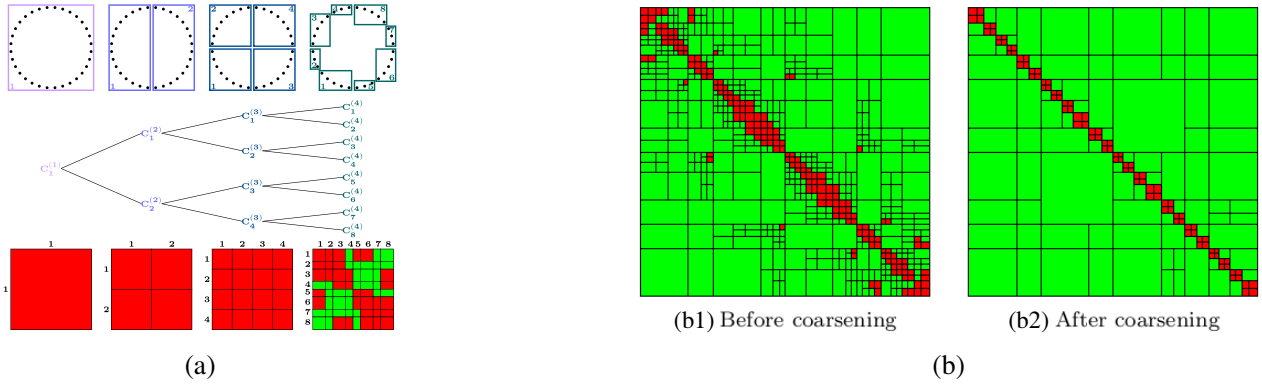

Figure 2. Initial construction of an $\mathcal{H}$-matrix and coarsening. (a) Clustering of a circle discretized by 32 points and the resulting $\mathcal{H}$-matrix. The green blocks can be compressed contrary to the red ones. (b) Effect of coarsening of an $\mathcal{H}$-matrix.

3.1.2. Coarsening

In a second step, a purely algebraic and geometry-independent recompression, known as coarsening, allows to optimize and simplify the hierarchical structure, as represented in Figure 2(b).

3.2. Assembly of Block Matrix: Numerical Results

We begin the numerical study by the assembly of the matrix F. The test case used in this work is a PCF with many holes, as illustrated in Figure 3. We will consider the matrices F_2^H and F_4^H corresponding

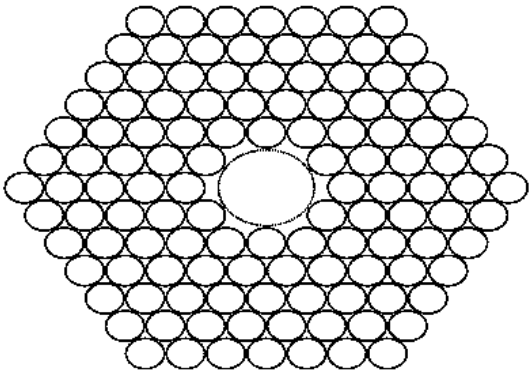

Figure 3. PCF with 121 holes for numerical tests.

to the $\mathcal{H}$-matrix building for, respectively, the problem with 2 unknowns (μ^E, μ^H) and 4 unknowns $(\mu^E, \mu^H, \sigma_i^E, \sigma_i^H)$. The approach without compression will be denoted as F_2^d and F_4^d as the direct approach for, respectively, the problem with 2 unknowns and 4 unknowns.

The numerical tests in this section correspond to several discretizations of the fiber illustrated in Figure 3 with the following parameters: the free space wavelength is $\lambda = 1.51\,\mu$m. Each inclusion has a diameter of $2.603\,\mu$m, and the RI of the glass matrix is 1.45.

Figures 4(a) and 4(b) show the evolution of the assembly time and the required memory vs the total number of unknowns N by taking into account several values of the accuracy parameter ϵ_{ACA} (see Subsection 3.1).

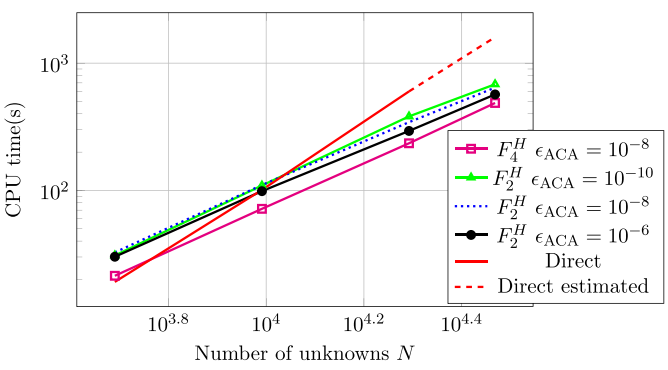

(a) CPU time

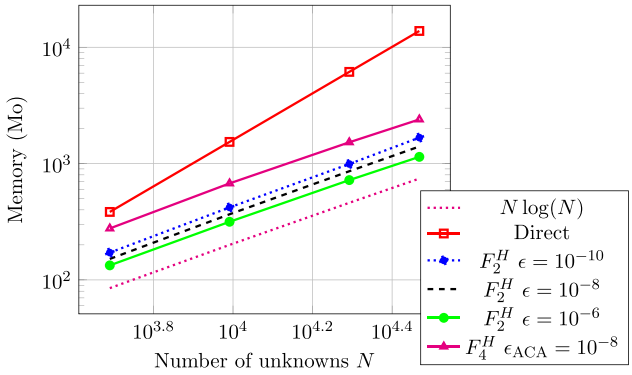

(b) Memory

Figure 4. Study relatively to the accuracy parameter. (a) CPU time. (b) Memory.

Table 1. Accuracy for the computation of f at some distance of a root.

ϵ_{ACA}	10^{-10}	10^{-8}	10^{-6}
$E_{\mathcal{H}}$	$1.376\ 10^{-8}$	$1.480\ 10^{-6}$	$1.255\ 10^{-4}$

In both cases, we observe that we are close to the theoretical curve in $\mathcal{O}(N\log(N))$ for the $\mathcal{H}$-matrix assembly that becomes more efficient when the size of the problem increases. Note that the numerical tests are more focused on the strategy with 2 unknowns, which is the most efficient if we consider the assembly and solution set. For estimating the accuracy obtained in Table 1, we define the error on the solution as

$$E_{\mathcal{H}} = \|u_{\mathcal{H}} - u_{ref}\|_2$$

where $u_{\mathcal{H}}$ is the solution of the linear system solved with the compressed hierarchical matrix, and u_{ref} is the solution of the linear system without compression. The right-hand side is the random matrix $\boldsymbol{\psi} \in \mathbb{C}^{n\times p}$ defined previously. The same matrix was taken for the entire numerical experiences. Parameters of the solution (next section) are taken very accurate to focus the error study on the compression accuracy.

For these tests, we choose a particular point which is one of the simulation points considered in the solution method [14] of the nonlinear problem. This point is not close to the singularity.

As a result, ϵ_{ACA} provides a control on the resulting error $E_{\mathcal{H}}$, even if it cannot be exactly guaranteed that $E_{\mathcal{H}} \leqslant \epsilon_{\text{ACA}}$.

4. H-LU SOLVER AND PRECONDITIONING

4.1. Theory

One of the advantages of the $\mathcal{H}$-matrix format is the ability to perform an LU decomposition directly in a hierarchical format [17]. This operation will be denoted as H-LU, and its accuracy is controlled by a parameter ϵ_{LU}. This factorization allows a fast "direct" solution, or the construction of an efficient preconditioner by applying H-LU to a coarser approximation of the matrix [18, 19]. This preconditioner will be denoted by P-HLU in the results, and its accuracy is controlled by a parameter ϵ_{prec}.

4.2. Some Numerical Tests

4.2.1. Accuracy of the $\mathcal{H}$-Matrix Solver

We now turn our focus to the efficiency of the $\mathcal{H}$-matrix solver (or preconditionner) which is involved in the nonlinear solution process. The computed error is still relative to the solution obtained by the direct solver without compression. Here, direct or iterative solver corresponds to the strategy used to solve $F^{-1}(n_{\mathit{eff}})\boldsymbol{\psi}$ in (16). The error for the direct H-LU solver is controlled by ϵ_{LU}. The considered iterative method is a Krylov solver for multiple right-hand sides denoted as MGCR and defined in [20]; its error is controlled by the tolerance parameter ϵ_{solver}. This iterative solver is preconditioned by a P-HLU approach whose accuracy ϵ_{prec} is set to 10^{-4}. It can be seen in Tables 2 and 3 that the $\mathcal{H}$-matrix solver is relatively efficient in maintaining a "good" accuracy on the cost function proportional to the compression accuracy ϵ_{ACA}.

Table 2. Accuracy for the computation of f at some distance of a root.

$\epsilon_{\text{solver}} = \epsilon_{\text{LU}}$	10^{-10}	10^{-8}	10^{-6}	10^{-4}
$E_{\mathcal{H}}$ H-LU	$6.309\ 10^{-8}$	$6.761\ 10^{-6}$	$8.061\ 10^{-4}$	$1.213\ 10^{-1}$
$E_{\mathcal{H}}$ P-HLU+MGCR	$1.408\ 10^{-10}$	$1.590\ 10^{-8}$	$2.856\ 10^{-7}$	$1.142\ 10^{-4}$

Table 3. Accuracy for the computation of f at some distance of a root.

ϵ_{ACA}	10^{-10}	10^{-8}	10^{-6}
ϵ_{solver}	10^{-8}	10^{-6}	10^{-4}
$E_{\mathcal{H}}$ P-HLU+MGCR	$1.590\ 10^{-8}$	$1.507\ 10^{-6}$	$1.656\ 10^{-4}$

4.2.2. Some Strategies for the Solver Computation Times

It is noted here that the layout of the blocks has a large influence on the computation process. Our tests suggest that the best strategy will be to keep the full blocks at the bottom part of the matrix. For

the system defined by (13), it leads, for instance, to the following ordering

$$\begin{bmatrix} W_i & 0 & B_1 & 0 \\ 0 & W_i & 0 & B_1 \\ W_e & \frac{c_2}{c_1}B_3 & -\frac{c_0}{c_1}B_2 & 0 \\ \frac{c_2}{c_4}B_3 & W_e & 0 & -\frac{c_3}{c_4}B_2 \end{bmatrix} \cdot \begin{bmatrix} \mu^E \\ \mu^H \\ \sigma_i^E \\ \sigma_i^H \end{bmatrix} = 0. \tag{17}$$

One explanation could be that these particular orderings minimize the initial fill-in of the matrix during the implementation of the H-LU algorithm.

Table 4 summarizes the computation times and the corresponding number of iterations in the iterative solver with the P-HLU preconditioner, depending on the accuracy on the preconditioner.

Table 4. Computation time with the reordered matrix. $\epsilon_{\text{ACA}} = 10^{-8}$ and $\epsilon_{\text{solver}} = 10^{-6}$. rhs denotes right-hand side.

ϵ_{prec}	10^{-6}	10^{-5}	10^{-4}	10^{-3}
Niter (20 rhs)	40	60	100	198
CPU Multi GCR (s)	4.77 s	6.96 s	11.31 s	22.16 s
CPU P-HLU-Prec (s)	87.53 s	76.22 s	66.25 s	55.60 s
CPU P-HLU-Prec + MGCR (s)	92.30 s	83.18 s	77.56 s	77.76 s

As a result, it seems that the optimal choice for computation times would be to set the accuracy around 10^{-4} for the preconditioner. It is also interesting to note that 10^{-5} and 10^{-3} are numerically not so far apart, implying that the computation time does not strongly depend on the accuracy of the preconditioner.

4.2.3. Comparison with the Direct Solver Approach

We now consider the performances in terms of computation times of the $\mathcal{H}$-matrix solver, used as a direct solver ($\epsilon_{\text{LU}} = 10^{-8}$) or as a preconditioner ($\epsilon_{\text{prec}} = 10^{-4}$), to that of the direct uncompressed solution which is used here as the reference.

As illustrated in Figure 5, the H-LU solver becomes faster than the direct solver and with a complexity of $\mathcal{O}(N\log(N))$, for size N between $10,000$ and $20,000$ unknowns with an advantage for the preconditionning strategy.

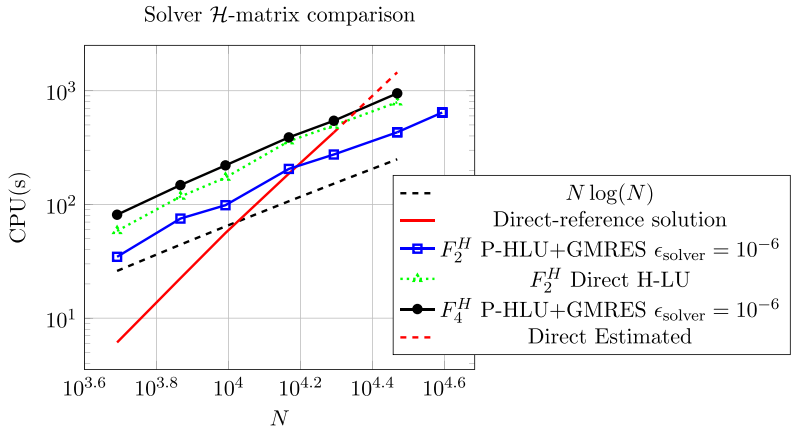

Figure 5. Direct vs $\mathcal{H}$-matrix solver.

5. SOLUTION OF THE NONLINEAR PROBLEM

In the following numerical examples, N_d denotes the number of discretization points considered on one "hole" of the PCF (see Figure 3).

5.1. Error Study on the Nonlinear Eigenvalue Problem

In this last section, we investigate the effect of the accuracy of the compression on the final solution of the nonlinear problem related to PCF from Figure 3 (see Table 5).

Table 5. Accuracy of the nonlinear problem with $N_d = 30$ except for the central hole where $N_d = 86$.

ϵ_{ACA}	ϵ_{solver}	Solution 1	Solution 2
10^{-11}	10^{-9}	$0.984516211638 + \text{i}3.39941801\,10^{-8}$	$0.9845161199599 + \text{i}3.39958587\,10^{-8}$
10^{-10}	10^{-8}	$0.984516211637 + \text{i}3.39908256\,10^{-8}$	$0.9845161199599 + \text{i}3.39942039\,10^{-8}$
10^{-9}	10^{-7}	$0.984516211620 + \text{i}3.39583076\,10^{-8}$	$0.9845161620018 + \text{i}3.40187262\,10^{-8}$
10^{-8}	10^{-6}	$0.984516211700 + \text{i}3.43882404\,10^{-8}$	$0.9845161619644 + \text{i}3.45863975\,10^{-8}$
10^{-7}	10^{-5}	$0.984516210338 + \text{i}3.39416590\,10^{-8}$	$0.9845161624987 + \text{i}3.56678295\,10^{-8}$
10^{-6}	10^{-4}	$0.984516190377 + \text{i}1.53222381\,10^{-8}$	$0.9845161652082 + \text{i}4.43654762\,10^{-8}$
0.	0.	$0.984516211638 + \text{i}3.3993574\,10^{-8}$	$0.984516119958 + \text{i}3.39956748\,10^{-8}$

As a result, the accuracy on the computed n_{eff} follows the solution parameters ϵ_{ACA} and ϵ_{solver} settings.

5.2. A Large Example Computation

Finally, we implement the $\mathcal{H}$-matrix solver on the following large-size PCF comprising 294 holes, as illustrated in Figure 6.

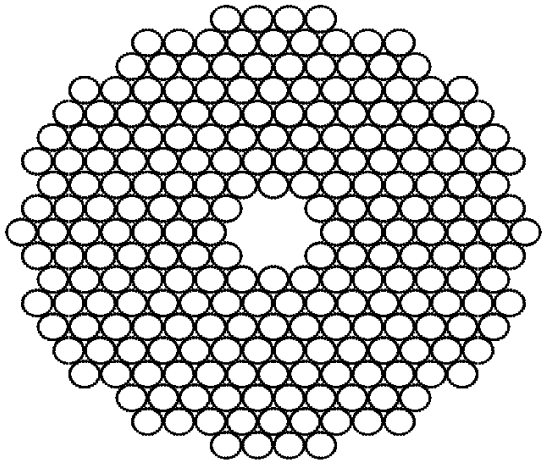

Figure 6. Large Hollow-core simulation.

Global dimensions and properties of the material for this example are taken the same as described in the previous PCF example.

Table 6. n_{eff} solution of the nonlinear problem.

N_d	N	F_2 direct	F_2^H	N	F_4^H
16	4704	$0.9842819532 + 7.80531\,10^{-5}$i	$0.9842819533 + 7.80531\,10^{-5}$i	9408	$0.9842819533 + 7.80531\,10^{-5}$i
20	11760	$0.9840368193 + 5.90451\,10^{-6}$i	$0.9840368195 + 5.90443\,10^{-6}$i	23520	$0.9840368193 + 5.90446\,10^{-6}$i
24	14112	$0.9839110693 + 2.41149\,10^{-8}$i	$0.9839110693 + 2.41081\,10^{-8}$i	28224	$0.9839110693 + 2.41129\,10^{-8}$i
30	17640	$0.9839178418 + 2.11891\,10^{-8}$i	$0.9839178418 + 2.11956\,10^{-8}$i	35280	$0.9839178418 + 2.11929\,10^{-8}$i
34	19992		$0.9839190263 + 2.13405\,10^{-8}$i	39984	$0.9839190262 + 2.13181\,10^{-8}$i
40	23520		$0.9839190191 + 2.13172\,10^{-8}$i	47040	$0.9839190191 + 2.13128\,10^{-8}$i

Table 6 illustrates the convergence of our method with F_2^H and F_4^H strategies, and with respect to the mesh density employed.

For validation purposes, we compute the direct solution for the maximum number of unknowns allowed by the memory.

As illustrated by the solution in Table 6, "very" good correspondence between the solutions with several strategies is achieved. The $\mathcal{H}$-matrix solver allows now to increase the size of the problem and the accuracy for the final PCF solution.

6. CONCLUSION

In this paper, we have proposed a methodology to apply hierarchical methods to efficiently solve a system of coupled BEM equations involved in a nonlinear solver for PCF applications. Although it is penalized by a large constant due to the complex nature of the problem, the proposed solution allows to recover the usual complexity in $\mathcal{O}(N\log(N))$ for both computation times and memory and then be able to solve nonlinear problems of large sizes, which would otherwise be impossible.

REFERENCES

1. Russel, P., "Photonic crystal fibers," *Science*, Vol. 299, No. 5605, 358–362, Jan. 2003.
2. Vassallo, C., *Optical Waveguide Concepts*, Elsevier, Amsterdam, 1991.
3. Chiou, Y. P., Y. C. Chiang, C. H. Lai, C. H. Du, and H. C. Chang, "Finite difference modeling of dielectric waveguides with corners and slanted facets," *Journal of Lightwave Technology*, Vol. 27, No. 12, 2077–2086, Dec. 2009.
4. Brechet, F., J. Marcou, D. Pagnoux, and P. Roy, "Complete analysis of the characteristics of propagation into photonic crystal fibers by the finite element method," *Optical Fiber Technology*, Vol. 6, 181–191, Apr. 2000.
5. Selleri, S., L. Vincetti, L. A. Cucinotta, and M. Zoboli, "Complex FEM modal solver of optical waveguides with PML boundary conditions," *Optical Quantum Electronics*, Vol. 33, 359–371, 2001.
6. Monro, T. M., D. J. Richardson, N. G. R. Broderick, and P. J. Bennett, "Modeling large air fraction holey optical fibers," *Journal of Lightwave Technology*, Vol. 18, No. 1, 50–56, Jan. 2000.
7. Alivizatos, E. G., I. D. Chremmos, N. L. Tsitsas, and N. K. Uzunoglu, "Green's-function method for the analysis of propagation in holey fibers," *Journal of Optical Society of America*, Vol. 21, No. 5, 847–857, May 2004.
8. White, T. P., B. T. Kuhlmey, R. C. Mcphedran, D. Maystre, G. Renversez, C. Martijn de Sterke, and L. C. Botten, "Multipole method for microstructured optical fibers. I. Formulation," *Journal of Optical Society of America*, Vol. 19, No. 10, 2322–2330, Oct. 2002.
9. Lu, W. and Y. Y. Lu, "Efficient boundary integral equation method for photonic crystal fibers," *Journal of Lightwave Technology*, Vol. 30, No. 11, 1610–1616, Jun. 2012.

10. Lu, W. and Y. Y. Lu, "Efficient high order waveguide mode solvers based on boundary integral equations," *Journal of Computational Physics*, Vol. 272, 507–525, Apr. 2014.
11. Song, J. and W. C. Chew, "Multilevel fast-multipole algorithm for solving combined field integral equations of electromagnetic scattering," *Microwave and Optical Technology Letters*, Vol. 10, 14–19, 1995.
12. Bebendorf, M., "Approximation of boundary element matrices," *Numerische Mathematik*, Vol. 86, 565–589, 2000.
13. Grasedyck, L. and W. Hackbusch, "Construction and arithmetics of H-matrices," *Computing*, Vol. 70, 295–334, 2003.
14. Beyn, W.-J., "An integral method for solving nonlinear eigenvalue problems," *Linear Algebra and Its Applications*, Vol. 436, No. 10, 3839–3863, 2012.
15. Kress, R., "On the numerical solution of a hypersingular integral equation in scattering theory," *Journal of Computational and Applied Mathematics*, Vol. 61, 345–360, Jun. 1995.
16. Cheng, R., W. Y. Crutchfield, M. Doery, and L. Greengard, "Fast, accurate integral equation methods for the analysis of photonic crystal fibers. I: Theory," *Optics Express*, Vol. 12, No. 16, 3791–3805, 2004.
17. Bebendorf, M., "Hierarchical matrices — A means to efficiently solve elliptic boundary value problems," Lecture Notes in Computational Science and Engineering, Springer, 2008.
18. Bebendorf, M., "A hierarchical LU decomposition-based preconditioners for BEM," *Computing*, Vol. 74, 225–247, 2005.
19. Daquin, P., R. Perrussel, and J.-R. Poirier, "Hybrid cross approximation for the electric field integral equation," *Progress In Electromagnetics Research M*, Vol. 75, 79–90, 2018.
20. Soudais, P., "Iterative solution of a 3-D scattering problem from arbitrary shaped multidielectric and multiconducting bodies," *IEEE Transactions on Antennas and Propagation*, Vol. 42, No. 7, 954–959, Jul. 1994.